Applied Catalysis B: Environmental 257 (2019) 117885

Contents lists available at ScienceDirect

Applied Catalysis B: Environmental

journal homepage: www.elsevier.com/locate/apcatb

Mixed iron-manganese oxides as redox catalysts for chemical looping–oxidative dehydrogenation of ethane with tailorable heat of reactions

Seif Yusuf, Vasudev Haribal, Daniel Jackson, Luke Neal, Fanxing Li*

Department of Chemical and Biomolecular Engineering, North Carolina State University, 911 Partners Way, Raleigh, NC, 27695-7905, United States

ARTICLE INFO

Keywords:
Oxidative dehydrogenation
Chemical looping
Ethane
Ethylene

ABSTRACT

The chemical looping-oxidative dehydrogenation (CL-ODH) of ethane is investigated in this study. In CL-ODH, a redox catalyst donates its lattice oxygen to combust hydrogen formed from ethane dehydrogenation (ODH reactor). The reduced redox catalyst is then transferred to a separate reactor (regenerator), where it is re-oxidized with air. Typically, the ODH step is endothermic, due to the high endothermicity to reduce the redox catalyst. This energy demand is met through sensible heat carried by the redox catalyst from the regenerator, which operates at a higher temperature. This temperature difference between the two reactors leads to exergy losses. We report an Fe-Mn redox catalyst showing tunable exothermic heat of reduction. Promotion with Na_2WO_4 resulted in high ethylene yields due to the suppression of surface Fe/Mn. ASPEN Plus® simulations indicated that Fe-Mn redox catalysts can lower the temperature difference between the two reactors. This can lead to efficiency improvements for CL-ODH.

1. Introduction

Ethylene is a heavily utilized commodity chemical for the production of important compounds such as polyethylene, ethylene oxide, dichloroethane, ethylbenzene, and acetaldehyde [1]. Worldwide production of ethylene is projected to more than triple by the year 2050 relative to the 2013 production level of 150 million tonnes/year [2]. Due to the recent increase in shale gas production, ethylene production from ethane, the second most abundant component in shale gas, has become particularly attractive [3]. The predominant production route for ethylene is the steam cracking of ethane, in which ethane is pyrolyzed at elevated temperature in the presence of steam diluent [1]. This endothermic process requires fired heaters to supply the necessary high heating rates, resulting in substantial CO_2 and NO_x emissions from the combustion of carbonaceous fuels such as methane [4]. Additional energy demands arise from downstream compression and separation units such that, in total, more than 16 GJ of energy is required to produce one ton of ethylene through steam cracking [1]. Thermodynamic equilibrium limitations on ethane conversion and coke formation in steam crackers also limit the performance of steam crackers [5].

Ethylene production through direct oxidative dehydrogenation (ODH) of ethane has been explored to replace steam cracking [6–10]. ODH utilizes a co-feed of ethane and oxygen, the latter of which combusts hydrogen and removes equilibrium limitations. The resulting reaction is exothermic ($\Delta H = -105$ kJ/mol at 850 °C):

$$C_2H_6 + \tfrac{1}{2}\,O_2 \rightarrow C_2H_4 + H_2O \quad (1)$$

Ethane ODH with oxygen co-feed has been extensively studied in terms of both catalyst development and mechanistic investigations [11–19]. Satisfactory ethylene yields (> 40%) were reported in numerous studies [20–29], with a MoVTeNbO catalyst showing an ethylene selectivity of 81% and ethylene yield of 75% [30]. Although these results are highly promising, conventional ODH faces a few practical challenges. For instance, this method introduces the potential safety hazard of mixing ethane and gaseous oxygen, and air separation units upstream of the ODH reactor are costly and energy-intensive to build and operate. Downstream separation and purification of the ethylene product stream is also complex and energy intensive [31]. To overcome the challenges of co-feeding ethane ODH, we investigated a two-step chemical looping ODH (CL-ODH) scheme, which addresses many of the challenges facing catalytic ethane ODH [31–35]. In CL-ODH, a redox catalyst donates oxygen from its crystal lattice to convert ethane to ethylene and water. Subsequently, the reduced catalyst is transferred to the regenerator where it is re-oxidized in air and sent back to the ODH reactor, completing the redox cycle. Acting as an oxygen carrier, the

* Corresponding author.
E-mail address: fli5@ncsu.edu (F. Li).

https://doi.org/10.1016/j.apcatb.2019.117885
Received 10 April 2019; Received in revised form 23 May 2019; Accepted 18 June 2019
Available online 19 June 2019
0926-3373/

redox catalyst can be repeatedly reduced and oxidized.

$$C_2H_6 + MeO_x \rightarrow C_2H_4 + MeO_{x-1} + H_2O \text{ (ODH reactor)} \quad (2)$$

$$MeO_{x\text{-}1} + 1/2O_2 \text{ (air)} \rightarrow MeO_x + \text{heat (Regenerator)} \quad (3)$$

There are several potential benefits of CL-ODH over traditional ODH: (i) CL-ODH avoids the safety issues inherent to co-feeding ethane and oxygen; and (ii) the use of an oxygen carrier eliminates the need for costly air separation units. In CL-ODH, process heat integration between the two reactors is accomplished through the direct heat transfer of the sensible heat in the oxygen carrier particles, resulting in reduced energy requirements. Experimental studies indicated that CL-ODH can result in higher single-pass yield of ethylene compared to thermal cracking [33–37]. ASPEN Plus® simulations further indicated that the CL-ODH scheme can reduce energy consumption and emissions by up to 82% compared to traditional steam cracking because of the selective combustion of hydrogen and lower demand for downstream separation [31].

Compared to conventional ODH in the presence of a heterogeneous catalyst, CL-ODH is comparatively less developed. Previous CL-ODH studies have examined redox catalysts containing vanadium and molybdenum [38–42], but the highest obtained ethylene yield was 38% with the majority of catalysts showing ethylene yields below 20%. Further concerns with toxicity, high material cost, and potential stability/sublimation issues may limit and attractiveness of V and Mo based redox catalysts. Manganese and iron oxides are alternative redox catalysts that are abundant, low-cost and relatively benign and each have been studied for chemical looping applications [43–49]. Mn oxides have been studied as oxygen carriers for chemical looping combustion (CLC) and chemical looping with oxygen uncoupling (CLOU) of methane and coal [43,44,46–48,50,51]. We have previously reported Mn-containing oxides such as mixed Mn-Mg and Mn-Si oxides for CL-ODH [32,34,35,52]. For instance, Mg_6MnO_8 exhibited a low ethylene selectivity of 14% at 850 °C and 3000hr^{-1} GHSV, but the selectivity was increased to 48.5% with a sodium pyrophosphate promoter and to 89.2% with a sodium tungstate (Na_2WO_4) promoter [34]. A manganese silicate oxygen carrier showed ethylene selectivity of 44.08% at 850 °C and 3000hr^{-1} GHSV, which increased to 63.33% with the addition of sodium tungstate [35]. The primary effect of Na_2WO_4 promotion was to decrease the CO_x selectivity, which was the primary undesired byproduct in CL-ODH [53]. For instance, CO_x selectivity dropped from 36.52% to 2.96% for manganese silicate redox catalysts and from 78.04% to 2.23% for Mg_6MnO_8 redox catalysts. Alkali metal oxide promotion also improved the selectivity of redox catalysts composed of Fe-containing perovskites [33,37]. Overall, alkali metal containing promoters, especially Na_2WO_4, have shown promise to improve the ethylene selectivity on various redox catalysts containing Mn and/or Fe oxides in CL-ODH.

It is noted that CL-ODH reactions carried out using the redox catalysts mentioned above are generally endothermic, with Mn_3O_4 redox catalysts showing an estimated heat of reaction of 118 kJ/mol C_2H_6 [36], which is comparable to thermal cracking (143 kJ/mol C_2H_6). Although this endothermicity would not affect the overall exothermicity of the two-step CL-ODH cycle, the energy demand in the ODH step does need to be satisfied by the sensible heat carried by the redox catalyst particles from the regenerator. Such heat integration requirements would dictate: (i) a large temperature difference between the ODH reactor and regenerator; and/or (ii) a high solids circulation rate. As such, CL-ODH operation can potentially be further optimized by developing CL-ODH redox catalysts with lower endothermicity for CL-ODH (Fig. 1). In this aspect, mixed Fe-Mn oxides are promising candidates considering their abilities for tunable and spontaneous oxygen release [54–57]. The present study investigates mixed Fe-Mn oxides as redox catalysts for the CL-ODH of ethane. Specifically, focuses were placed on the development of redox catalysts with less endothermic and potentially tunable CL-ODH heat of reactions while maintaining high activity and selectivity. It was determined that the best performing redox catalyst had a Fe-Mn molar ratio of 20–80. This heat of reduction of this catalyst was exothermic at all stages of reduction, and after promotion with Na_2WO_4, it was able to achieve an ethylene yield of 62.21% and a CO_x selectivity of 3.15%. ASPEN Plus® simulations indicate that Fe-Mn redox catalysts can decrease the temperature difference between the ODH and regenerator reactors and while having similar solid circulation rates as traditional coal chemical looping combustion (CLC) systems. The properties of this redox catalyst will allow for the further optimization of the CL-ODH process through additional energy savings.

2. Experimental

2.1. Redox catalyst synthesis

All redox catalysts were synthesized through a sol-gel procedure in order to obtain a redox catalyst with higher homogeneity. In this procedure, metal precursors (iron (III) nitrate nonahydrate (Sigma-Aldrich ACS reagent, $\geq$98% and manganese (II) nitrate tetrahdyrate (Sigma-Aldrich, $\geq$97.0%) and citric acid (Sigma Aldrich $\geq$99.5%) were dissolved in DI water. The citric acid to total cation molar ratio was 2.5 and the mixture was stirred at 50 °C for 30 min. Afterwards, ethylene glycol (Sigma Aldrich, anhydrous 99.8%) was added (ethylene glycol to citric acid molar ratio = 1.5) and the temperature was raised to 80 °C to complete the gelation process. The resulting mixture was dried overnight at 80 °C and then calcined in air at 450 °C for 3 h to decompose any nitrates and remove citric acid. Then the temperature was raised to 900 °C for 8 h in order to obtain the desired crystal phases. After calcination, the synthesized redox catalyst was sieved into 3 particles sizes: 850–425 μm, 425–250 μm, and < 250 μm. A total of three Fe-Mn molar ratios were synthesized: 20–80, 50-50 and 60–40.

Each of the base redox catalysts were promoted with sodium tungstate. The sieved redox catalyst particles were mixed with a water solution containing sodium tungstate dihydrate (Sigma Aldirch, 99.5%). The weight loading of sodium tungstate for all redox catalysts was 1.7 wt% on an Na basis. The promoted particles were then dried overnight at 80 °C, and then calcined in air at 900 °C for an additional 8 h. In this paper, un-promoted redox catalysts are designated by the Fe-Mn molar ratio (20–80, 50-50, and 60–40) and promoted redox catalysts are designated using the Fe-Mn molar ratio and Na_2WO_4 (20–80-Na_2WO_4, 50-50-Na_2WO_4, and 60-40-Na_2WO_4).

2.2. Ethane ODH experiments

The activity of the synthesized redox catalysts for the ODH of ethane was determined using a previously described reactor setup and gas chromatography analysis [35]. A U-tube reactor made of quartz with a 1/4″ O.D and 1/8″ I.D. was used for reaction testing. 0.5 g of redox catalyst particles was loaded into the bottom of the reactor and alumina grit (16 mesh) was used on both sides of the U-tube to prevent loss of redox catalyst particles and to reduce the gas residence time inside the heated reactor. In order to obtain thermal cracking (blank) measurements, a U-tube with only alumina grit was used.

The gas composition and flow rate inside the quartz U-tube reactor were controlled with mass flow controllers and a valve manifold. The overall GHSV during all pretreatment steps and reaction testing was 4500hr^{-1}. During the pretreatment step, the redox catalysts underwent 2 redox cycles which were comprised of a 3 min reduction step (80%/20% H_2/Ar) and a 3 min oxidation step (17%/83% O_2/Ar) at 900 °C. The pretreatment step resulted in a redox catalyst with stable chemical and physical properties. For ethane ODH reaction testing, the oxidation remained unchanged, but the reduction step was altered: a total of 5 ml of ethane was flown into the reactor (5 s injection of 80%/20% C_2H_6/Ar). In between each reduction and oxidation step during the pretreatment and ethane ODH reaction testing, 100% Ar was flown into the

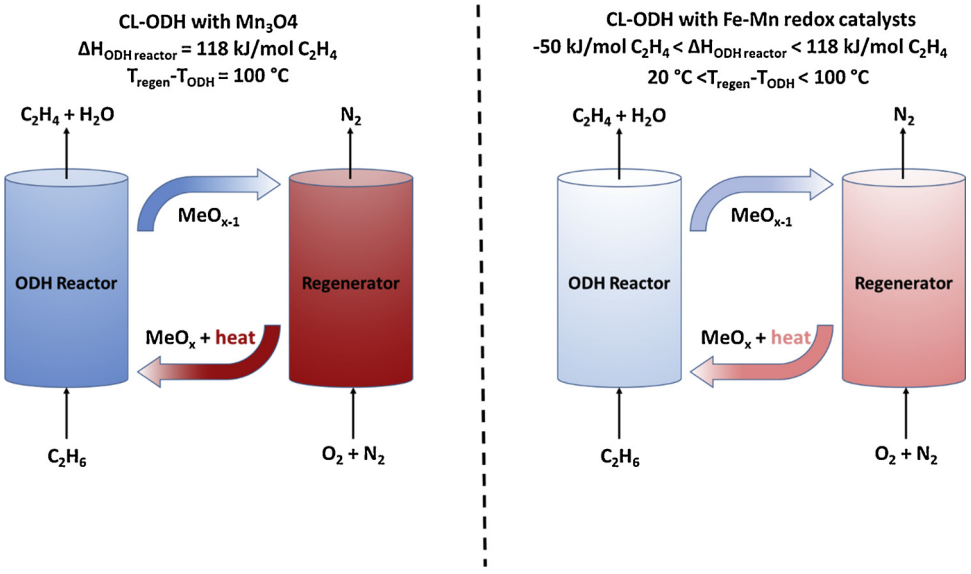

Fig. 1. CL-ODH scheme with Mn_3O_4 (left) and Fe-Mn redox catalysts (right).

reactor for 5 min. Ethane ODH reaction testing was performed at 850, 825, and 800 °C for all redox catalysts.

The products from the reduction step were collected in a gas bag and injected into a gas chromatograph (GC) for analysis. The GC was an Agilent 7890 Fast RGA with a flame ionization detector (FID) for hydrocarbon analysis and two thermal conductivity detectors for CO, CO_2, and H_2 analysis. A refinery gas standard (Agilent Part # 5190-0519) was used to calibrate the GC. Mass Spectroscopy analysis of the oxidation step did not show significant coking or tar formation, so a carbon mass balance was used to calculate ethane conversion and hydrocarbon product selectivity and yields. The product distribution was also used to calculate the amount of hydrogen formed during the reduction step and the amount of hydrogen converted to water. Formulas for product selectivity, yield and hydrogen conversion can be found below (n(x) refers to the total amount of carbon in species x measured by GC).

$$Ethane\ Conversion = 1 - \frac{n(Ethane)}{n(All\ carbon\ species)} \quad (4)$$

$$Selectivity\ (species\ x) = \frac{n(x)}{n(All\ carbon\ species) - n(ethane)} \quad (5)$$

$$Ethylene\ yield = Ethane\ Conversion * Selectivity(Ethyelene) \quad (6)$$

$$H_2\ combustion = 1 - \frac{(H_2)_{out}}{(H_2)_{gen}} \quad (7)$$

2.3. XRD characterization

Powder X-ray Diffraction (XRD) was done to determine crystal phases present in freshly synthesized and post testing redox catalysts. The measurements were performed at room temperature with a Rigaku SmartLab X-ray Diffractometer. The radiation source was Cu Kα (λ = 0.1542 nm) and the diffractometer operated at 40 kV and 44 mA. XRD patterns between 10-80° (2Θ) were generated with a step size of 0.1° and a hold time of 2.5 s.

2.4. Surface area measurements

A Micromeritics ASAP 2020 was used to collect N_2 adsorption isotherms at 77 K. Before adsorption isotherms were generated, all redox catalysts were degassed at 473 K. Brunauer-Emmett-Teller (BET) theory was used to calculate surface areas from the measured adsorption isotherms.

2.5. TGA/DSC measurements

The heat of reduction of each of the redox catalysts was measured on a TA Instruments SDT Q600 Dual Thermogravimetric Analysis (TGA)/Differential Scanning Calorimetry (DSC) unit. First, fresh redox catalyst was loaded into the sample crucible and heated to 850 °C in a 10% O_2/Ar environment to clean the redox catalyst. Then, the 5 H_2/O_2 redox cycles were performed on the redox catalyst. In each cycle, the initial gas flow was 10% O_2/Ar. After 10 min, the gas flow was switched to 100% Ar for 10 min and then to 10% H_2/Ar for 10 min to reduce the redox catalyst. After another 10 min 100% Ar purge, the gas flow was switched to its initial conditions (10% O_2/Ar). This completed the redox cycle and allowed the redox catalyst to be re-oxidized. The heat flow curve was integrated using TA Instruments TRIOS software in order to determine the heat of reduction of each redox catalyst. A detailed explanation of the integration process can be found in the supporting information

2.6. XPS analysis

Fresh (as-synthesized) and cycled (more than 30 C_2H_6/O_2 redox cycles, cleaned in 17% O_2/Ar at 850 °C, held at 850 °C in an 100% Ar atmosphere for 1 h, and then cooled to room temperature in 100% Ar atmosphere) redox catalysts were analyzed using X-ray photoelectron spectroscopy (XPS). Both the near-surface atomic composition and the oxidation states of manganese and iron were determined for all measured redox catalysts. All analysis was performed using an Al anode and the XPS system was comprised of a Thermo-Fisher Alpha 110 hemispherical energy analyzer and a Thermo-Fischer XR3, 300 W dual-anode X-Ray source. The C1s peak (284.6 eV) was used to calibrate all spectra.

2.7. Process simulation

ASPEN Plus® is used to simulate the ODH reactor and analyze the effect of obtained heat flow in the Fe-Mn system on the solid circulation rates. The ODH reactor is represented by an RStoic rector model, using the product distribution obtained in the ethane ODH experiments. A sequential modular approach is used. The ODH reactor is operated at 850 °C. Fe_2O_3 is used as a representative solid with pure ethane as the feed. The heat of the reaction is balanced so that it matches the experimentally obtained ΔH values. Additional information is provided in the supporting information. The circulation rates of the CL-ODH system

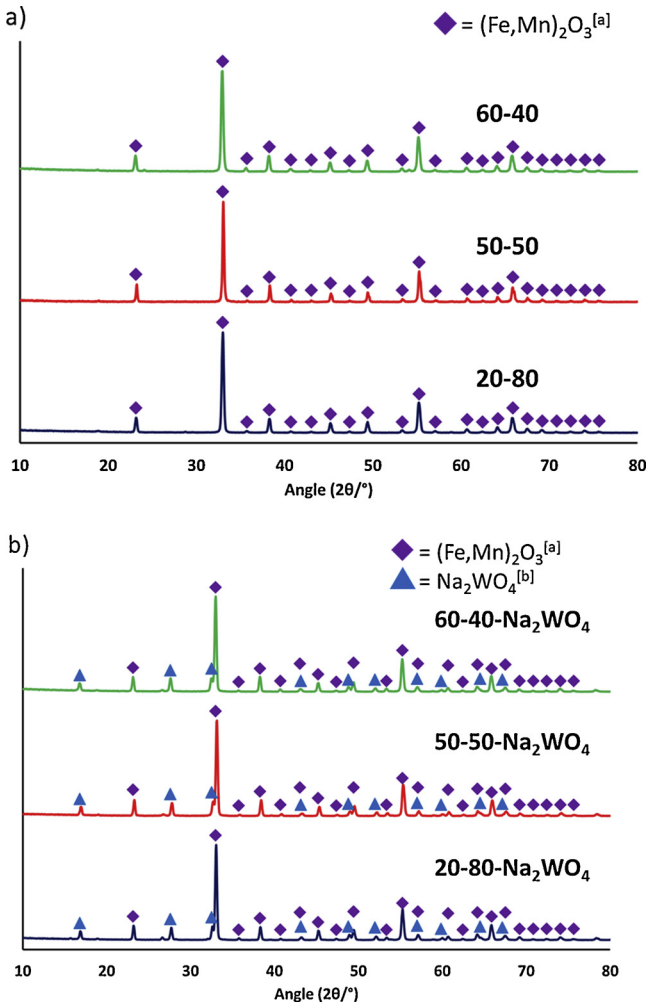

Fig. 2. XRD patterns of as-synthesized redox catalysts (a) un-promoted and (b) Na_2WO_4 promoted Fe:Mn oxide catalysts. [a]PDF# 01-075-0894 [b]PDF# 04-008-8508.

are compared with coal CLC systems, which are well studied.

3. Results and discussion

3.1. Redox catalyst characterization

Fig. 2 shows the XRD patterns for the freshly synthesized redox catalysts. The characteristic peaks for a bixbyite phase [$(Fe,Mn)_2O_3$ (PDF# 01-075-0894)] were observed on all un-promoted and promoted redox catalysts. The Na_2WO_4 (PDF#04-008-8508) phase was also seen on all of the promoted redox catalysts. No $(Fe,Mn)_3O_4$ spinel oxide phases, which represent a reduced form of mixed Fe-Mn oxides, were identified on any of the redox catalysts. The measured surface areas (Table 1) of the as-synthesized un-promoted redox catalysts are similar and after promotion with Na_2WO_4, the surface area for all redox catalysts decreases by around 50% in all cases.

Table 1
BET surface areas for the as-synthesized redox catalysts.

Redox Catalyst	Surface Area (m^2/g)
20-80	3.48
50-50	4.10
60-40	3.17
20-80-Na_2WO_4	1.75
50-50-Na_2WO_4	1.28
60-40-Na_2WO_4	1.47

3.2. ODH reaction testing

Ethane ODH results at 850 °C and a GHSV of $4500hr^{-1}$ for all synthesized redox catalysts are summarized in Fig. 3. All of the redox catalysts exhibited higher ethane conversions than thermal cracking (75.7–83.3% vs 62.9%) and had a H_2 conversion higher than 70% (which is desirable for the CL-ODH from an energy balance standpoint [31]). When comparing the un-promoted redox catalysts, the 20–80 redox catalyst showed the highest CO_x selectivity (50.7%) while the 50-50 and 60-40 redox catalysts had lower CO_x selectivity values (35.2 and 37.5% respectively). These results matched with previous literature, which have shown that Mn^{3+} oxides are active for the deep oxidation of hydrocarbons [58,59]. In previous studies [32,34,35], promotion with Na_2WO_4 caused a decrease in ethane and H_2 conversion, but the significant increase in ethylene selectivity led to an increase in ethylene yield. For all redox catalysts, the ethylene yields significantly increased after promotion with Na_2WO_4. The largest increase in ethylene yield was observed on the 20–80 redox catalyst (33.5% to 62.2%) and the 60-40-Na_2WO_4 redox catalyst demonstrated the highest ethylene yield (64.5%). H_2 conversion also decreased for all promoted redox catalysts, but ethane conversion only decreased for the 20–80-Na_2WO_4 redox catalyst (78.5% to 75.9%). The increase in ethane conversion on the 50-50-Na_2WO_4 and 60-40-Na_2WO_4 redox catalysts (75.9% to 79.6% and 75.7% to 83.3% respectively) is likely to be due to the densification of the promoted redox catalysts during reaction testing. This densification increased the effective gas residence time in the U-tube reactor, allowing for additional ethane conversion. In Fig. 4, the effect of reaction temperature on ethylene and CO_x selectivity is shown. As expected, a decrease in reaction temperature caused a decrease in ethane conversion and increase in ethylene selectivity (Fig. 4a). With respect to ethylene yield, the 60-40-Na_2WO_4 redox catalyst was the best performing at all temperatures, but the yield differences are relatively small as can be seen from Fig. 4a. The small differences between the promoted redox catalysts decreased as the reaction temperature decreased. A slightly different trend is seen in CO_x selectivity values on the promoted redox catalysts (Fig. 4b). At 850 °C, the 20–80-Na_2WO_4 redox catalyst showed the lowest CO_x selectivity (3.2%) followed by the 50-50-Na_2WO_4 redox catalyst (4.8%) and finally the 60-40-Na_2WO_4 redox catalyst (5.8%). At all temperatures, the 20:80-Na_2WO_4 redox catalyst exhibited the lowest CO_x selectivity. Due to the similar ethylene yield and lower CO_x selectivity, the 20–80-Na_2WO_4 redox catalyst was determined to the best performing redox catalyst. Detailed reaction data for the 20–80-Na_2WO_4 redox catalyst at all reaction temperatures can be found in the supplementary information (Table S1)

The proposed CL-ODH scheme requires that the redox catalysts demonstrate a long lifetime. Therefore, extended redox cycling was performed on the 20–80-Na_2WO_4 redox catalyst (Fig. 5). As the redox catalyst undergoes additional redox cycles, the ethane conversion increased until reaching a steady value at cycle 35 (80.1%–90.0%). Over the first 35 cycles, there was also a decrease in ethylene selectivity (80.7%–72.2%), but the ethylene yield was relatively stable (64.6%–65.1%). There was also an increase in C3+ selectivity (8.5%–12.2%) and CO_x selectivity (3.3%–7.5%) while the methane selectivity was relatively stable (6.9%–7.1%). The overall C2+ selectivity, which represents the formation of value-added products, decreased by 4.8% over extended redox cycle testing (89.0%–84.2%). After cycle 35, no significant changes in these values were observed. These results indicated that the 20–80-Na_2WO_4 redox catalyst is potentially suitable for CL-ODH applications in terms of redox stability.

3.3. XPS analysis

XPS analysis was performed to determine the near surface atomic

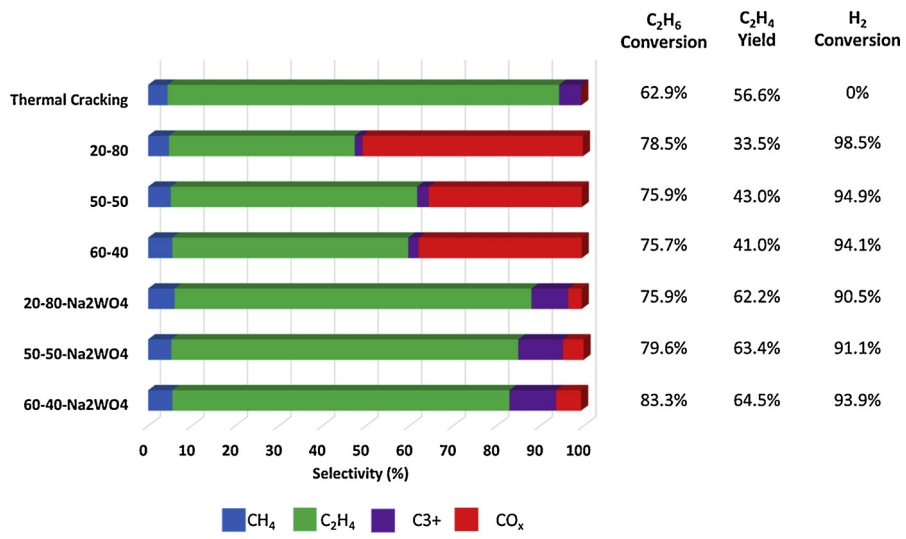

Fig. 3. Ethane ODH reaction data at 850 °C and GHSV = 4500hr^{-1} for thermal cracking (blank) and CL-ODH in the presence of the redox catalysts.

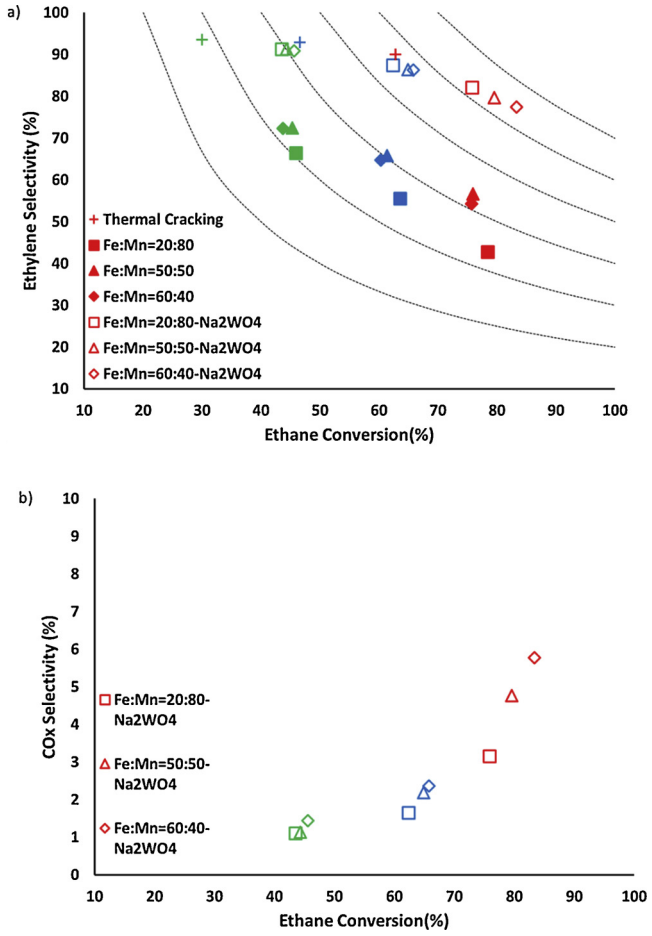

Fig. 4. Ethane ODH reaction data at varying temperatures a) Ethylene Selectivity vs ethane conversion and b) CO_x selectivity vs ethane conversion (Green: 800 °C, Blue: 825 °C, Red: 850 °C and GHSV = 4500hr^{-1}). (For interpretation of the references to colour in this figure legend, the reader is referred to the web version of this article).

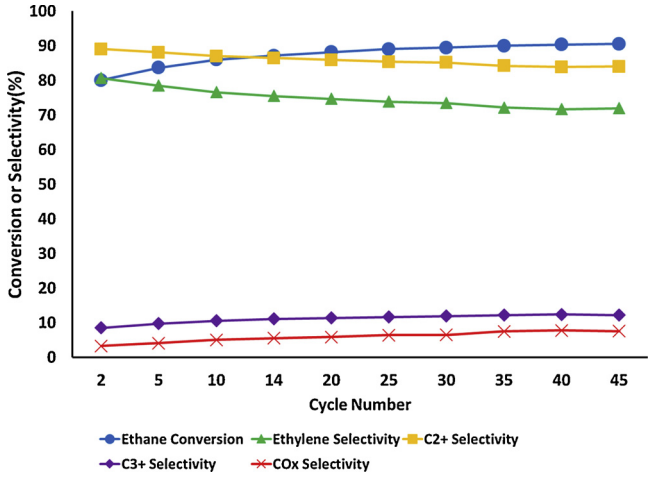

Fig. 5. Extended redox cycle testing on 20–80-Na_2WO_4 redox catalyst at 850 °C and GHSV = 4500hr^{-1}.

Table 2
Near-surface atomic % on fresh and cycled catalysts (oxygen and carbon free basis).

Catalyst	Fe%	Mn%	Na%	W%
20-80: fresh	13.21	86.79	0	0
20-80: cycled	16.05	83.95	0	0
20-80-Na_2WO_4: fresh	7.88	52.53	26.47	13.11
20-80-Na_2WO_4: cycled	5.79	37.98	23.09	33.14

composition and oxidation states of iron and manganese species on the 20–80 and 20–80-Na_2WO_4 redox catalysts. As described earlier in the experimental section, 2 versions of each redox catalysts were analyzed: fresh and cycled. The near surface atomic percentages (normalized to a carbon and oxygen free basis), for all analyzed redox catalysts are shown in Table 2. On the fresh 20–80 redox catalyst, the surface atomic percentages were similar to the bulk molar ratio and after cycling there were no significant changes in the surface composition. On the fresh 20–80-Na_2WO_4 redox catalyst, both Na and W are enriched as seen on previously studied Mg_6MnO_8 and manganese silicates based redox catalysts [34,35]. The as-synthesized Na and W enrichment factor (observed surface % divided by bulk %) were 4.92 and 4.87 respectively. Also, there were twice as many Na atoms observed as W atoms on the near surface of the fresh 20–80-Na_2WO_4 redox catalyst. The is the same ratio of Na to W in sodium tungstate. When comparing the fresh and cycled 20–80 redox catalysts there were no substantial differences. The cycled 20–80-Na_2WO_4 redox catalyst had slightly lower

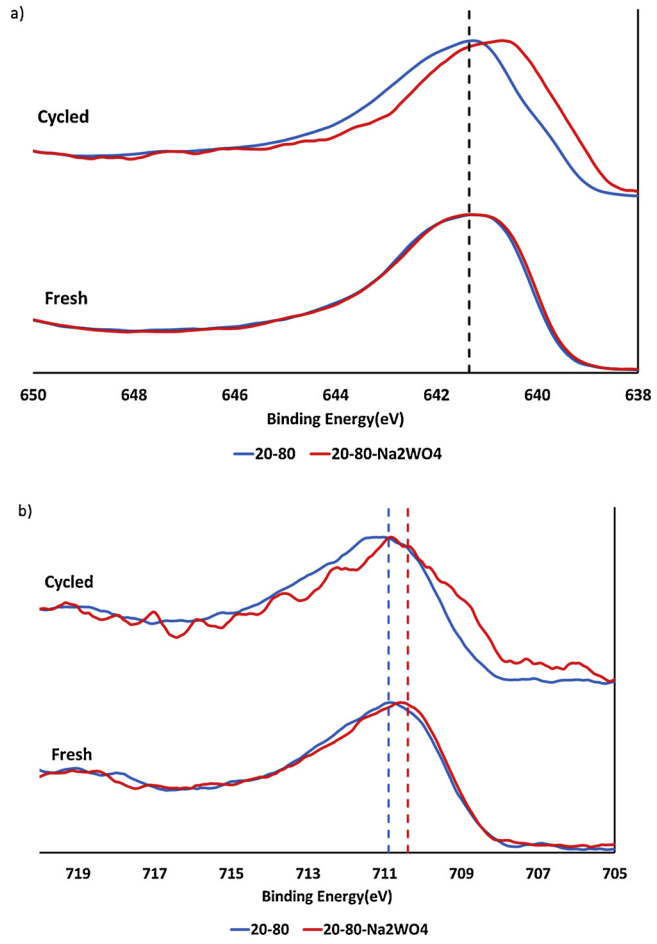

Fig. 6. XPS spectra of a) Mn $2p_{3/2}$ peak and b) Fe $2p_{3/2}$ of fresh and cycled redox catalysts.

Na and Fe surface atomic percentages when compared to the fresh 20–80-Na_2WO_4 redox catalyst, but there was a significant enrichment of W and loss of Mn which led to a decrease in the Na to W atomic surface ratio (~2 to 0.7). The decrease in this ratio is due to the loss of the Na_2WO_4 phase which was confirmed through XRD analysis of the cycled 20–80-Na_2WO_4 redox catalyst (Fig. S1). After ethane ODH reaction testing, the Na_2WO_4 phase was replaced by and (Fe,Mn)WO_4, $NaFe(WO_4)_2$ and $NaFeO_2$ phases. Unlike previously studied redox catalysts [34,35,53], the increase in ethylene yield was not due to the formation of a physical layer of Na_2WO_4 around the base redox catalyst. Instead, the primary reason for increased selectivity of the promoted redox catalysts was likely to be the suppression of Mn and Fe cations, and hence nonselective oxygen species, through the enrichment of Na and W on the surface of the redox catalyst. Further analysis of the XPS spectra, as discussed below, provides additional insights on the change in redox catalyst selectivity before and after Na_2WO_4 promotion.

The Mn $2p_{3/2}$ peak for the fresh and cycled redox catalysts can be seen in Fig. 6a. For the fresh redox catalysts, both the 20–80 and 20–80-Na_2WO_4 had an overall Mn $2p_{3/2}$ peak position of 641.2 eV which is consistent with Mn^{3+}. The cycled 20–80 redox catalyst had the same peak position as the fresh 20–80 redox catalyst, but the peak position shifted down by 0.5 eV for the cycled 20–80-Na_2WO_4 redox catalyst, indicating a slight decrease in the oxidation state for the near surface Mn cation. This shift was also seen on previously studied Mg_6MnO_8 redox catalysts [34]. Fig. 6b compares the Fe $2p_{3/2}$ spectra for the fresh and cycled redox catalysts. On fresh 20–80 redox catalyst, the Fe $2p_{3/2}$ peak was at 710.9 eV which corresponds to Fe^{3+} and promotion with Na_2WO_4, caused the Fe $2p_{3/2}$ peak to shift down by 0.5 eV. When comparing the fresh and cycled redox catalysts, there were no changes observed in the Fe $2p_{3/2}$ peak positions. While small differences in the Fe and Mn oxidation states were observed on the Na_2WO_4 promoted redox catalysts, the primary effect of the Na_2WO_4 promoter is the decrease in Fe and Mn and enrichment of Na and W species on the surface of the redox catalyst leading to increases in ethylene yield. This matches with previously observed results which indicated that the over oxidation of methane, ethane and other hydrocarbon species can be suppressed when both sodium and tungsten are present on the surface of the redox catalyst [34,35,53,60–62].

3.4. Heat of reaction analysis

A potential challenge for CL-ODH is the endothermic reaction that occurs in the ODH reactor [31]. Our previous studies indicate that ethane ODH on Na_2WO_4 promoted Mn oxide redox catalysts proceeds via ethane cracking in parallel with selective hydrogen combustion [34]. Even though the overall two-step CL-ODH process is exothermic, the endothermic reduction of the redox catalyst with H_2 in the ethane conversion step makes the ODH reactor endothermic for all the redox catalysts reported to date. The necessary heat for the ODH reactor is supplied from the circulation of the redox catalysts through the regenerator. In one potential configuration with Mg_6MnO_8 based redox catalyst, the operating temperature of the regenerator needs to be 100 °C higher than the ODH reactor. Since the re-oxidation of the redox catalysts is exothermic, this temperature difference allows thermal energy be carried back to the ODH reactor through sensible heat of the redox catalysts. If the heat of reaction in the ODH reactor was less endothermic, the heat requirements of the ODH reactor would be easier to meet. This can lead to (i) decreased redox catalyst circulation rate; and/or (ii) decreased temperature differences between the two reactors. Both can result in additional capital and energy savings for CL-ODH. With this in mind, dual TGA/DSC measurements were performed to determine the heat of reduction of the mixed Fe-Mn oxides to assist the identification of redox catalysts with decreased endothermicity for ethane conversion. The average heat of reduction determined by dual TGA/DSC measurements are summarized in Table 3.

Table 3 also included the estimated heat of reduction calculated from HSC Chemistry assuming the redox catalyst was reduced from the spinel phase to the monoxide phase. This assumption was based of TGA measurements, which indicated that the reduction of the bixbyite to the spinel phase was irreversible and the sample primarily cycled between spinel and monoxide phases (Fig. S2). The transition from the bixbyite to the spinel phase was also seen on XRD spectra of the redox catalysts after the TGA/DSC measurements (Fig. S3).

As can be seen from Table 3, there was good agreement between the DSC results and HSC calculations. As the iron content of the redox catalysts increases, the heat of reduction became more endothermic. This was because the reduction of Fe_3O_4 to FeO with H_2 is endothermic (28.85 kJ/mol O) while the reduction of Mn_3O_4 to MnO is exothermic (-25.38 kJ/mol O). Only the 20–80 redox catalyst had the desired exothermic heat of reduction, but for CL-ODH applications, it would be better to compare how the heat of reduction changes as the catalyst is reduced. In Fig. 7, the cumulative average heat flow per mol of O released is plotted versus the weight of O donated normalized by the initial redox catalyst weight (see supporting information file). All of the redox catalysts initially had a highly exothermic heat flow. As

Table 3
Heat of reduction from dual TGA/DSC measurements and HSC chemistry.

Redox Catalyst	Dual TGA/DSC (kJ/mol O)	HSC Chemistry (kJ/ mol O)
20-80	−14.26	−14.53
50-50	2.40	1.74
60-40	4.75	7.16

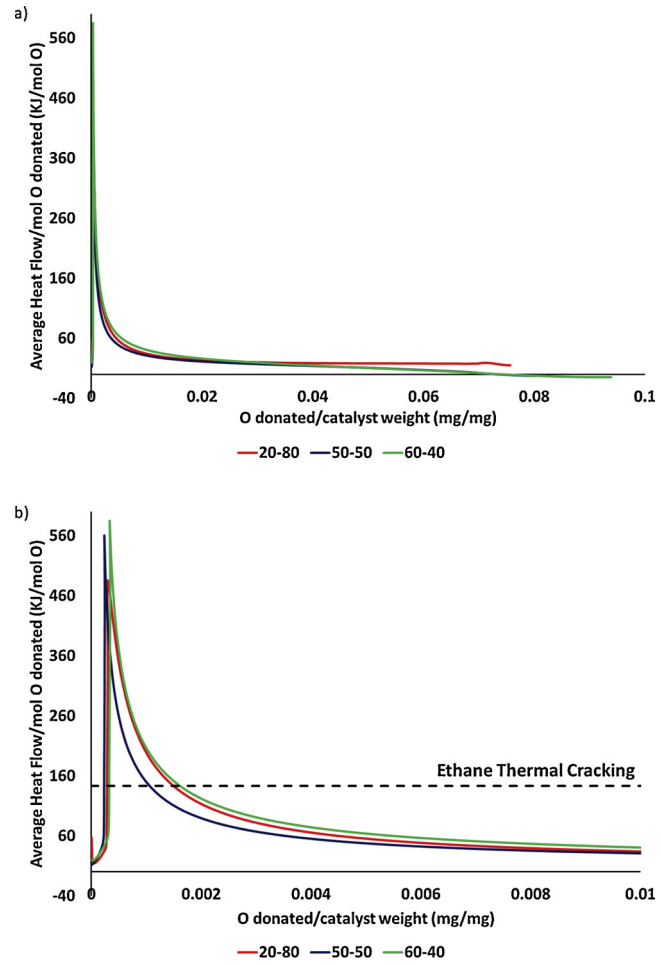

Fig. 7. Cumulative average heat flow per mol of O donated for the un-promoted redox catalysts. a) The complete integrated range for each redox catalyst. b) The first weight percent donated for each the redox catalysts. Positive average heat flow is exothermic and negative average heat flow is endothermic.

additional lattice oxygen was donated, the cumulative average heat flow became less exothermic (Fig. 6a). The 60-40 redox catalyst had the highest exothermic peak, which is likely due to the hematite phase that was detected from XRD measurements (Fig. S3). As expected from the previous heat flow data, the average heat flow for the 20–80 redox catalyst was exothermic regardless of the amount of oxygen donated while the average heat flows for the 50-50 and 60-40 redox catalysts become endothermic after extensive oxygen donation. All redox catalysts were initially able to offset the endothermicity for ethane cracking (143 kJ/mol C_2H_6 at 850 °C) at low oxygen donation. Therefore, we focused on the initial reduction of each of the redox catalysts (Fig. 7b). Here it was seen that the 60-40 redox catalyst was able to donate the most amount of lattice oxygen (0.16 wt%) while maintaining exothermic or heat neutral during the CL-ODH step. This is followed with 20–80 (0.14 wt%) and 50-50 (0.12 wt%) redox catalysts. Despite the higher exothermicity during the initial reduction, the 60-40 redox catalyst was a less desirable candidate than the 20–80 redox catalyst from a process development standpoint.

Since CL-ODH in principle just decouples an overall exothermic ODH reaction into two-steps, the regenerator reactor would supply the heat, if necessary, to offset the endothermic reaction in the ODH reactor. In Fig. 8, the heat of reaction in the ODH and regenerator reactors utilizing the 20–80 redox catalyst are plotted versus the oxygen capacity of the 20–80 redox catalysts. For the first 0.14% of the oxygen capacity, the heat of reaction in the ODH reactor was exothermic, so all of the heat from the regenerator could be used to generate low pressure

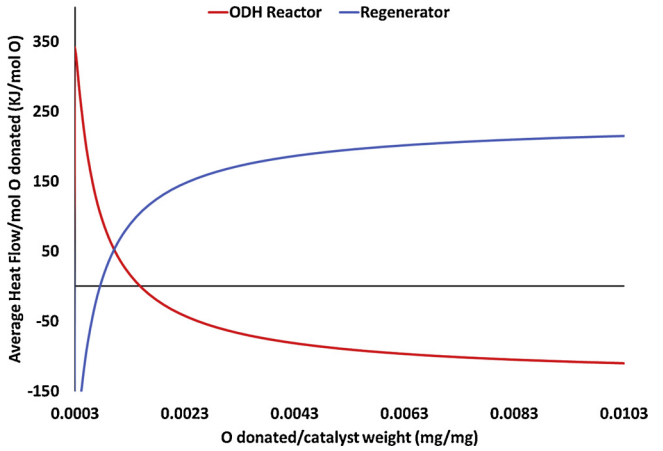

Fig. 8. Average heat flow for the ODH and regenerator reactor for the 20–80 redox catalyst. Positive average heat flow is exothermic and negative average heat flow is endothermic.

steam [31]. Additional oxygen donation leads to an overall endothermic ODH reactor, but at 1% oxygen capacity donated, only 30.8% of the heat from the regenerator reactor is needed for the ODH reactor (111 kJ/mol O vs 360 kJ/mol O). As such, both the heat of reaction and ethane ODH results indicate that the 20–80-Na_2WO_4 is promising for a CL-ODH process. It is therefore further studied in an ASPEN Plus® model.

3.5. Process analysis

The CL-ODH system is proposed to be operated in a circulating fluidized bed (CFB) scheme, where the redox catalyst circulation rate (R_{cat}) is crucial as the redox catalyst supplies the necessary heat to offset the endothermicity of the ODH reactor. There are two important factors which govern the circulation rate of redox catalyst in the system: 1) oxygen release from the redox catalyst supplying the heat via selective hydrogen combustion (ΔH_{SHC}) and 2) ΔT between the ODH reactor and regenerator providing sensible heat. Optimization of these factors can allow for adiabatic operation of the ODH reactor, providing a more efficient operation, which adds to the energy savings for the process.

The Fe-Mn system provides an exothermic SHC, as shown in Figs. 7 and 8, which can reduce the overall ΔH of the ODH reactor. This can lower the required R_{cat} values (mass of redox catalyst circulated/hr). To analyze the effects of the observed heat flows, the ODH reactor is simulated using ASPEN Plus®. For the ODH reactor, with a fixed ΔH_{SHC} and oxygen capacity, the temperature of the regenerator (or redox catalyst feed) is varied, till the ODH reactor reaches 850 °C. This leads to a data set of projected solids circulation rate (R_{cat}) vs ΔT (between the regenerator and ODH reactor).

R_{cat} values (ktonne/hr) are calculated for a 1500 MW_{Th} ethylene production plant which corresponds to an annual ethylene production of approximately 1 million tonnes. The selected points are mapped on Fig. 9, plotted as R_{cat} vs ΔT. CLC of coal has been well documented in literature and is used as a reference [55,63–66]. Ilmenite is chosen as the reference oxygen carrier for the CLC systems. Based on the available literature, circulation rates for a 1500 MW_{Th} capacity CLC system are also plotted in Fig. 9.

As one would anticipate, low oxygen release (or oxygen capacity utilized) for CL-ODH would correspond to large solids circulation rates mainly due to the needs to supply adequate lattice oxygen for ethane conversion. This leads to high circulation rates and low temperature difference between reactors. Increasing oxygen release from the Fe-Mn oxides can lower solids circulation from an oxygen supply standpoint. However, this leads to increased endothermicity in the CL-ODH reactor

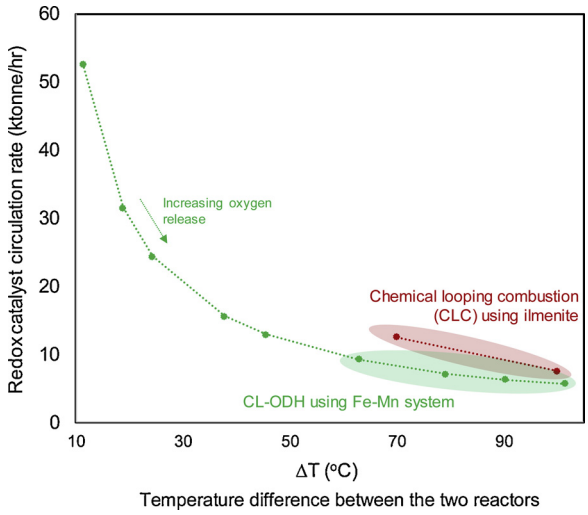

Fig. 9. Projected solid circulation rates of the Fe-Mn redox catalyst system (20–80) for CL-ODH and the corresponding reactor temperature differences (at 1500 MW_{th} feedstock processing capacity). Corresponding data on coal chemical looping combustion (CLC) system are also shown as references [63].

and hence requires a higher reactor temperature difference. Overall, the tunable heat of reaction for mixed Fe-Mn oxide redox catalysts, as a function of oxygen release, allows the flexibility of adjusting reactor temperature differences and solids circulating rates. Moreover, under a similar reactor temperature difference, the projected solids circulation rate for CL-ODH is comparable or slightly lower than that required for CLC of coal, indicating its potential technical feasibility.

4. Conclusion

This study explored mixed iron manganese redox catalysts for the CL-ODH of ethane. Three molar ratios (Fe-Mn) were studied: 20–80, 50-50, and 60-40. XRD analysis indicated that all as-synthesized redox catalysts contained a mixed $(Fe,Mn)_2O_3$ phase. Ethane ODH reaction testing showed that after promotion with Na_2WO_4, the 20–80 redox catalyst achieved high ethylene yields (62.21%) and a low selectivity towards CO_x species (3.15%). XPS results showed that both sodium and tungsten were enriched on the surface of the 20–80-Na_2WO_4 redox catalyst. Continuous redox cycling induced the formation of (Fe,Mn) WO_4, $NaFe(WO_4)_2$ and $NaFeO_2$ phases in addition to the mixed Fe-Mn oxides which acted as the oxygen carrying phases. These results indicated that near surface tungsten and sodium synergistically suppressed the deep oxidation of hydrocarbons. Dual TGA/DSC measurements indicated that a 20–80 redox catalyst had an exothermic heat flow during reduction indicating that it can help offset the endothermic nature of ethane cracking. ASPEN Plus® simulations indicate that the Fe-Mn redox catalyst can significantly lower the solids solid circulation rate when compared to traditional coal CLC processes. Moreover, the circulation rate and reactor temperature difference is tunable by varying the amount of oxygen extraction from the redox catalyst. Overall, the 20–80-Na_2WO_4 redox catalyst is a promising oxygen carrier for a CL-ODH process and can lead to reductions in energy consumption and emissions from ethylene production.

Acknowledgements

We acknowledge the funding support from the US Department of Energy (RAPID Subaward DE- EE007888-05-6), the US National Science Foundation (Award No. CBET- 1,604,605) and the Kenan Institute of Engineering, Technology, and Science at NC State University.

Appendix A. Supplementary data

Supplementary material related to this article can be found, in the online version, at doi:https://doi.org/10.1016/j.apcatb.2019.117885.

References

[1] Ullmann's Encyclopedia of Industrial Chemistry, Wiley-VCH Verlag GmbH & Co. KGaA, Weinheim, Germany, 2000.
[2] F. Ausfelder, A. Bazzanella, H. VanBracki, R. Wilde, C. Beckmann, R. Mills, E. Rightor, C. Tam, N. Trudeau, P. Botschek, Technology Roadmap Energy and GHG Reductions in the, (2013), pp. 1–60.
[3] J.J.H.B. Sattler, J. Ruiz-Martinez, E. Santillan-Jimenez, B.M. Weckhuysen, Catalytic dehydrogenation of light alkanes on metals and metal oxides, Chem. Rev. 114 (2014) 10613–10653.
[4] T. Ren, M. Patel, K. Blok, Olefins from conventional and heavy feedstocks: Energy use in steam cracking and alternative processes, Energy 31 (2006) 425–451.
[5] M.M. Bhasin, Is True Ethane Oxydehydrogenation Feasible? Top. Catal. 23 (2003) 145–149.
[6] C.A. Gärtner, A.C. van Veen, J.A. Lercher, Oxidative dehydrogenation of ethane: common principles and mechanistic aspects, ChemCatChem. 5 (2013) 3196–3217.
[7] R. Burch, R. Swarnakar, Oxidative dehydrogenation of ethane on vanadium-molybdenum oxide and vanadium-niobium-molybdenum oxide catalysts, Appl. Catal. 70 (1991) 129–148.
[8] E.A. Mamedov, V. Cortés Corberán, Oxidative dehydrogenation of lower alkanes on vanadium oxide-based catalysts. The present state of the art and outlooks, Appl. Catal. A Gen. 127 (1995) 1–40.
[9] M.A. Bañares, Supported metal oxide and other catalysts for ethane conversion: a review, Catal. Today 51 (1999) 319–348.
[10] S. Gaab, J. Find, T.E. Müller, J.A. Lercher, Kinetics and mechanism of the oxidative dehydrogenation of ethane over Li/Dy/Mg/O/(Cl) mixed oxide catalysts, Top. Catal. 46 (2007) 101–110.
[11] M. Abello, M. Gomez, O. Ferretti, Mo/γ-Al2O3 catalysts for the oxidative dehydrogenation of propane, Appl. Catal. A Gen. 207 (2001) 421–431.
[12] E. Heracleous, M. Machli, A.A. Lemonidou, I.A. Vasalos, Oxidative dehydrogenation of ethane and propane over vanadia and molybdena supported catalysts, J. Mol. Catal. A Chem. 232 (2005) 29–39.
[13] B. Solsana, A. Dejoz, T. Garcia, P. Concepcion, J. Nieto, M. Vazquez, M. Navarro, Molybdenum–vanadium supported on mesoporous alumina catalysts for the oxidative dehydrogenation of ethane, Catal. Today 117 (2006) 228–233.
[14] H. Zhu, D.C. Rosenfeld, D.H. Anjum, V. Caps, J.-M. Basset, Green synthesis of Ni-Nb oxide catalysts for low-temperature oxidative dehydrogenation of ethane, ChemSusChem. 8 (2015) 1254–1263.
[15] L. Ji, J. Liu, Excellent promotion by lithium of a lanthanum-calcium oxide catalyst for oxidative dehydrogenation of ethane to ethane, Chem. Commun. (Camb.) (1996) 1203–1203.
[16] B. Fu, J. Lu, P.C. Stair, G. Xiao, M.C. Kung, H.H. Kung, Oxidative dehydrogenation of ethane over alumina-supported Pd catalysts. Effect of alumina overlayer, J. Catal. 297 (2013) 289–295.
[17] H.H. Kristoffersen, H. Metiu, Molten LiCl Layer Supported on MgO: Its Possible Role in Enhancing the Oxidative Dehydrogenation of Ethane, J. Phys. Chem. C. 119 (2015) 8681–8691.
[18] C.A. Gärtner, A.C. van Veen, J.A. Lercher, Oxidative dehydrogenation of ethane on dynamically rearranging supported chloride catalysts, J. Am. Chem. Soc. 136 (2014) 12691–12701.
[19] D. Dogu, K.E. Meyer, A. Fuller, S. Gunduz, D.J. Deka, N. Kramer, A.C. Co, U.S. Ozkan, Effect of lanthanum and chlorine doping on strontium titanates for the electrocatalytically-assisted oxidative dehydrogenation of ethane, Appl. Catal. B Environ. 227 (2018) 90–101.
[20] J.M.L. Nieto, P. Botella, P. Concepción, A. Dejoz, M.I. Vázquez, Oxidative dehydrogenation of ethane on Te-containing MoVNbO catalysts, Catal. Today (2004) 241–245.
[21] P. Botella, E. García-González, A. Dejoz, J.M. López Nieto, M.I. Vázquez, J. González-Calbet, Selective oxidative dehydrogenation of ethane on MoVTeNbO mixed metal oxide catalysts, J. Catal. 225 (2004) 428–438.
[22] Q. Xie, L. Chen, W. Weng, H. Wan, Preparation of MoVTe(Sb)Nb mixed oxide catalysts using a slurry method for selective oxidative dehydrogenation of ethane, J. Mol. Catal. A Chem. 240 (2005) 191–196.
[23] C.P. Kumar, S. Gaab, T.E. Müller, J.A. Lercher, Oxidative dehydrogenation of light alkanes on supported molten alkali metal chloride catalysts, Top. Catal. 50 (2008) 156–167.
[24] B. Tope, Y. Zhu, J.A. Lercher, Oxidative dehydrogenation of ethane over Dy2O3/MgO supported LiCl containing eutectic chloride catalysts, Catal. Today 123 (2007) 113–121.
[25] A.S. Bodke, D. Henning, L.D. Schmidt, S.S. Bharadwaj, J.J. Maj, J. Siddall, Oxidative dehydrogenation of ethane at millisecond contact times: effect of H2 addition, J. Catal. 191 (2000) 62–74.
[26] A.S. Bodke, D.A. Olschki, L.D. Schmidt, E. Ranzi, High selectivities to ethylene by partial oxidation of ethane, Science 285 (1999) 712–715 80-..
[27] E. Heracleous, A. Lemonidou, Ni–Nb–O mixed oxides as highly active and selective catalysts for ethene production via ethane oxidative dehydrogenation. Part I: Characterization and catalytic performance, J. Catal. 237 (2006) 162–174.
[28] Y.S. Yun, M. Lee, J. Sung, D. Yun, T.Y. Kim, H. Park, K.R. Lee, C.K. Song, Y. Kim, J. Lee, Y.-J. Seo, I.K. Song, J. Yi, Promoting effect of cerium on MoVTeNb mixed

oxide catalyst for oxidative dehydrogenation of ethane to ethylene, Appl. Catal. B Environ. 237 (2018) 554–562.
[29] B. Sarkar, R. Goyal, L.N. Sivakumar Konathala, C. Pendem, T. Sasaki, R. Bal, MoO3 nanoclusters decorated on TiO2 nanorods for oxidative dehydrogenation of ethane to ethylene, Appl. Catal. B Environ. 217 (2017) 637–649.
[30] J.M.L. Nieto, P. Botella, M.I. Vázquez, A. Dejoz, The selective oxidative dehydrogenation of ethane over hydrothermally synthesised MoVTeNb catalysts, Chem. Commun. (Camb.) (2002) 1906–1907.
[31] V.P. Haribal, L.M. Neal, F. Li, Oxidative dehydrogenation of ethane under a cyclic redox scheme – process simulations and analysis, Energy 119 (2017) 1024–1035.
[32] P. Novotný, S. Yusuf, F. Li, H.H. Lamb, Oxidative dehydrogenation of ethane using MoO3/Fe2O3 catalysts in a cyclic redox mode, Catal. Today. 317 (2018) 50–55, https://doi.org/10.1016/j.cattod.2018.02.046.
[33] Y. Gao, L.M. Neal, F. Li, Li-Promoted LaxSr2-xFeO4-δ Core-Shell Redox Catalysts for Oxidative Dehydrogenation of Ethane under a Cyclic Redox Scheme, ACS Catal. 6 (2016) 7293–7302.
[34] S. Yusuf, L.M. Neal, F. Li, Effect of promoters on manganese-containing mixed metal oxides for oxidative dehydrogenation of ethane via a cyclic redox scheme, ACS Catal. 7 (2017) 5163–5173.
[35] S. Yusuf, L. Neal, V. Haribal, M. Baldwin, H.H. Lamb, F. Li, Manganese silicate based redox catalysts for greener ethylene production via chemical looping – oxidative dehydrogenation of ethane, Appl. Catal. B Environ. 232 (2018) 77–85.
[36] L.M. Neal, S. Yusuf, J.A. Sofranko, F. Li, Oxidative dehydrogenation of ethane: a chemical looping approach, Energy Technol. 4 (2016) 1200–1208.
[37] Y. Gao, F. Haeri, F. He, F. Li, Alkali Metal-Promoted La $_x$ Sr $_{2-x}$ FeO $_{4-\delta}$ Redox Catalysts for Chemical Looping Oxidative Dehydrogenation of Ethane, ACS Catal. 8 (2018) 1757–1766.
[38] S. Al-Ghamdi, M. Volpe, M.M. Hossain, H. de Lasa, VOx/c-Al2O3 catalyst for oxidative dehydrogenation of ethane to ethylene: desorption kinetics and catalytic activity, Appl. Catal. A Gen. 450 (2013) 120–130.
[39] A.H. Elbadawi, M.S. Ba-Shammakh, S. Al-Ghamdi, S.A. Razzak, M.M. Hossain, Reduction kinetics and catalytic activity of VOx/γ-Al2O3-ZrO2 for gas phase oxygen free ODH of ethane, Chem. Eng. J. 284 (2016) 448–457.
[40] S.N. Khadzhiev, N.Y. Usachev, I.M. Gerzeliev, V.P. Kalinin, V.V. Kharlamov, E.P. Belanova, A.V. Kazakov, S.A. Kanaev, T.S. Starostina, Ethane conversion involving lattice oxygen of oxide systems, Pet. Chem. U S S R 55 (2015) 640–644.
[41] S.N. Khadzhiev, N.Y. Usachev, I.M. Gerzeliev, E.P. Belanova, V.P. Kalinin, V.V. Kharlamov, A.V. Kazakov, S.A. Kanaev, T.S. Starostina, A.Y. Popov, Oxidative dehydrogenation of ethane to ethylene in a system with circulating microspherical metal oxide oxygen carrier: 1. Synthesis and study of the catalytic system, Pet. Chem. U S S R 55 (2015) 651–654.
[42] M.Y. Khan, S. Al-Ghamdi, S.A. Razzak, M.M. Hossain, H. de Lasa, Fluidized bed oxidative dehydrogenation of ethane to ethylene over VOx/Ce-γAl2O3 catalysts: reduction kinetics and catalyst activity, Mol. Catal. 443 (2017) 78–91.
[43] A. Shafiefarhood, A. Stewart, F. Li, Iron-containing mixed-oxide composites as oxygen carriers for Chemical looping with Oxygen Uncoupling (CLOU), Fuel 139 (2015) 1–10.
[44] A. Shafiefarhood, J. Zhang, L.M. Neal, F. Li, M. Uenishi, M. Kimura, T. Okamoto, N. Hamada, T.-L. Hsieh, A. Tong, Z. Sun, L.-S. Fan, Rh-promoted mixed oxides for "low-temperature" methane partial oxidation in the absence of gaseous oxidants, J. Mater. Chem. A Mater. Energy Sustain. 5 (2017) 11930–11939.
[45] T. Mattisson, A. Lyngfelt, H. Leion, Chemical-looping with oxygen uncoupling for combustion of solid fuels, Int. J. Greenh. Gas Control. 3 (2009) 11–19.
[46] N. Galinsky, M. Sendi, L. Bowers, F. Li, CaMn1-xBxO3-δ(B = Al, V, Fe, Co, and Ni) perovskite based oxygen carriers for chemical looping with oxygen uncoupling (CLOU), Appl. Energy 174 (2016) 80–87.
[47] N. Galinsky, A. Mishra, J. Zhang, F. Li, Ca1−xAxMnO3 (A=Sr and Ba) perovskite based oxygen carriers for chemical looping with oxygen uncoupling (CLOU), Appl. Energy 157 (2015) 358–367.
[48] A. Mishra, N. Galinsky, F. He, E.E. Santiso, F. Li, Perovskite-structured AMn x B 1−x O 3 (A = Ca or Ba; B = Fe or Ni) redox catalysts for partial oxidation of methane, Catal. Sci. Technol. 6 (2016) 4535–4544.
[49] N.L. Galinsky, A. Shafiefarhood, Y. Chen, L. Neal, F. Li, Effect of support on redox stability of iron oxide for chemical looping conversion of methane, Appl. Catal. B Environ. 164 (2015) 371–379.
[50] T. Mattisson, Materials for chemical-looping with oxygen uncoupling, ISRN chem, Eng. 2013 (2013) 1–19.
[51] V.P. Haribal, F. He, A. Mishra, F. Li, Iron-doped BaMnO3for hybrid water splitting and syngas generation, ChemSusChem. 10 (2017) 3402–3408.
[52] J.A. Sofranko, F. Li, L. Neal, Oxygen Transfer Agents for the Oxidative Dehydrogenation of Hydrocarbons and Systems and Processes Using the Same, WO2016049144 (2016).
[53] S. Yusuf, L. Neal, Z. Bao, Z. Wu, F. Li, Effects of sodium and tungsten promoters on Mg $_6$ MnO 8 -Based core–shell redox catalysts for chemical looping—oxidative dehydrogenation of ethane, ACS Catal. (2019) 3174–3186.
[54] G. Azimi, H. Leion, T. Mattisson, A. Lyngfelt, Chemical-looping with oxygen uncoupling using combined Mn-Fe oxides, testing in batch fluidized bed, Energy Procedia 4 (2011) 370–377.
[55] Y. Larring, C. Braley, M. Pishahang, K.A. Andreassen, R. Bredesen, Evaluation of a mixed Fe–Mn oxide system for chemical looping combustion, Energy Fuels 29 (2015) 3438–3445.
[56] R. Pérez-Vega, A. Abad, F. García-Labiano, P. Gayán, L.F. de Diego, M.T. Izquierdo, J. Adánez, Chemical Looping Combustion of gaseous and solid fuels with manganese-iron mixed oxide as oxygen carrier, Energy Convers. Manage. 159 (2018) 221–231.
[57] P. Moldenhauer, A. Serrano, F. García-Labiano, L.F. de Diego, M. Biermann, T. Mattisson, A. Lyngfelt, Chemical-looping combustion of kerosene and gaseous fuels with a natural and a manufactured Mn–Fe-Based oxygen carrier, Energy Fuels 32 (2018) 8803–8816.
[58] L.E. Cadus, O. Ferretti, Highly effective molybdena–manganese catalyst for propane oxidative dehydrogenation, Catal. Letters 69 (2000) 199–202.
[59] Q. Ge, B. Zhaorigetu, C. Yu, W. Li, H. Xu, Oxidative dehydrogenation of ethane and propane over Mn-based catalysts, Catal. Letters 68 (2000) 59–62.
[60] S. Ji, Surface WO4 tetrahedron: the essence of the oxidative coupling of methane over M_W_Mn/SiO2 catalysts, J. Catal. 220 (2003) 47–56.
[61] A. Palermo, J.P. Holgado Vazquez, R.M. Lambert, New efficient catalysts for the oxidative coupling of methane, Catal. Letters 68 (2000) 191–196.
[62] Y.T. Chua, A.R. Mohamed, S. Bhatia, Oxidative coupling of methane for the production of ethylene over sodium-tungsten-manganese-supported-silica catalyst (Na-W-Mn/SiO2), Appl. Catal. A Gen. 343 (2008) 142–148.
[63] J. Ströhle, M. Orth, B. Epple, Design and operation of a 1 MWth chemical looping plant, Appl. Energy 113 (2014) 1490–1495.
[64] J. Adánez, A. Abad, T. Mendiara, P. Gayán, L.F. de Diego, F. García-Labiano, Chemical looping combustion of solid fuels, Prog. Energy Combust. Sci. 65 (2018) 6–66.
[65] A. Abad, J. Adánez, L.F. de Diego, P. Gayán, F. García-Labiano, A. Lyngfelt, Fuel reactor model validation: assessment of the key parameters affecting the chemical-looping combustion of coal, Int. J. Greenh. Gas Control. 19 (2013) 541–551.
[66] A. Cuadrat, A. Abad, F. García-Labiano, P. Gayán, L.F. de Diego, J. Adánez, The use of ilmenite as oxygen-carrier in a 500 Wth Chemical-Looping Coal Combustion unit, Int. J. Greenh. Gas Control. 5 (2011) 1630–1642.